Large scale modelling of bubble formation and growth in a supersaturated liquid

Document status and date:
Published: 01/01/2017

Document Version:
Publisher's PDF, also known as Version of Record (includes final page, issue and volume numbers)

Please check the document version of this publication:

• A submitted manuscript is the version of the article upon submission and before peer-review. There can be important differences between the submitted version and the official published version of record. People interested in the research are advised to contact the author for the final version of the publication, or visit the DOI to the publisher's website.
• The final author version and the galley proof are versions of the publication after peer review.
• The final published version features the final layout of the paper including the volume, issue and page numbers.

Link to publication

Download date: 08. Jul. 2024

12th International Conference on CFD in Oil & Gas, Metallurgical and Process Industries
SINTEF, Trondheim, NORWAY
May 30th - June 1st, 2017

CFD 2017

LARGE SCALE MODELLING OF BUBBLE FORMATION AND GROWTH IN A SUPERSATURATED LIQUID

Alessandro BATTISTELLA[1], **Sander S.C. AELEN**[1], **Ivo ROGHAIR**[1]*,

Martin VAN SINT ANNALAND[1]

[1]Chemical Process Intensification, Department of Chemical Engineering and Chemistry, Eindhoven

University of Technology, Eindhoven, the Netherlands

* E-mail: i.roghair@tue.nl

ABSTRACT

Bubble formation due to supersaturation or superheating plays an important role in many different areas from boiling flows to reactions producing gases, such as in electrolytic processes or fermentation. The predominant mechanism for bubble formation is heterogeneous nucleation and, while it has been studied on the microscale, the effect of bubble nucleation on the large-scale performance of bubble column reactors is still scarcely investigated.

This work presents a modelling and simulation study on phase transition in bubble column reactors on the meso-scale using a discrete bubble model (DBM). The Discrete Bubble Model is an Euler-Lagrange model which tracks each bubble individually. The model has been extended to include the formation of bubbles due to the presence of supersaturation.

With this model, phase transition from liquid to gas in a supersaturated liquid has been studied for two cases: bubble formation on a solid surface and in a liquid bulk. The second case shows a larger number of bubbles formed, with a bigger size. The concentration front presents differences, as in the first case it shifts from a lower concentration at the bottom to the opposite.

To conclude, a starting point for simulations of phase transition due to supersaturation has been given in this work, showing that the choice of the mechanisms of bubble formation highly influence bubble densities, sizes and movements in the considered liquid.

Keywords: CFD, Bubble and droplet dynamics, Lagrangian methods, Multiphase heat and mass transfer. .

NOMENCLATURE

Greek Symbols

α Volume fraction, $[-]$

Γ Transport coefficient, $[\mathrm{m\,s^{-1}}]$

ζ Supersaturation ratio, $[-]$

θ Film thickness, $[\mathrm{m}]$

μ Dynamic viscosity, $[\mathrm{Pa\,s}]$

ρ Mass density, $[\mathrm{kilog/m^3}]$

σ Surface tension, $[\mathrm{N\,m^{-1}}]$

τ Stress tensor, $[\mathrm{N^2\,m^{-1}}]$

Φ Interphase momentum transfer, $[\mathrm{N\,m^{-1}}]$

Latin Symbols

A Surface area, $[\mathrm{m}]$.

C Model coefficients, $[-]$.

c Concentration, $[\mathrm{kmol\,m^{-1}}]$.

d_{eq} Equivalent diameter $d_{eq} = \left(\frac{1}{d_i} + \frac{1}{d_j}\right)^{-1}$, $[m]$.

D_b Bubble diameter, $[\mathrm{m}]$.

$\mathcal{D}$ Diffusion coefficient, $[\mathrm{m\,s^{-1}}]$.

Eö   Eötvös number Eö $= \frac{gD_b^2\rho}{\sigma}$, $[-]$.

E_b Bubble aspect ratio, $[-]$.

F   Force, $[\mathrm{N}]$.

g Gravitational acceleration, $[\mathrm{m^2\,s^{-1}}]$.

k_l Mass transfer coefficient, $[\mathrm{m\,s^{-1}}]$.

H Henry constant, $[-]$.

$\dot{M}$ Volume averaged interfacial mass transfer, $[\mathrm{kg\,s^{-1}\,m^{-1}}]$.

$\dot{m}$ Individual bubble mass transfer, $[\mathrm{kg\,s^{-1}}]$.

p Pressure, $[\mathrm{Pa}]$.

Re   Reynolds number Re $= \frac{\rho u D_b}{\mu}$, $[-]$.

R_b Radius, $[\mathrm{m}]$.

S Source term (reaction), $[\mathrm{kg\,s^{-1}\,m^{-1}}]$.

Sc   Schmidt number Sc $= \frac{\mu}{\rho\mathcal{D}}$, $[-]$.

Sh   Sherwood number Sh $= \frac{k_l D_b}{\mathcal{D}}$, $[-]$.

t Time, $[\mathrm{s}]$.

u   Liquid velocity, $[\mathrm{m\,s^{-1}}]$.

v   Gas velocity, $[\mathrm{m\,s^{-1}}]$.

V Volume, $[\mathrm{m}]$.

We   Weber number We $= \frac{\rho_l\left(v_{n,i}-v_{n,j}\right)^2 D_b}{\sigma}$, $[-]$.

Y^j Mass fraction of component j, $[-]$.

Sub/superscripts

b Bubble.

c Critical.

d Distorted.

i, j Indexes.

eff Effective.

l Liquid.

n Normal.

rel Relative.

s Saturation.

T Turbulent.

INTRODUCTION

Bubble columns, and in general bubbly flows, are widely used in industrial applications due to contact a gas and liquid in processes where reaction or heat/mass transport takes place between the phases. Despite the widespread applications of these systems, detailed knowledge on the complex interactions between hydrodynamics and mass/heat transport is still lacking, especially in the region of dense flows and

their effect on the large-scale performance of bubble column reactors. The use of Computational Fluid Dynamics (CFD) to model and study these systems is becoming more and more widespread resulting from large improvements in computational power. Different levels of detail (length scales) can be identified ranging from large Euler-Euler simulations to detailed DNS. At an intermediate level, Euler-Lagrange models, where each bubble is tracked individually in a Lagrangian manner, play an important role in gaining details on swarms with a large number of bubbles (van Sint Annaland *et al.*, 2003).

Phase transition as a consequence of supersaturation occurs in a variety of natural and industrial processes. For instance, a well known example is opening a bottle of soda: the sudden change in pressure creates a local supersaturation and bubbles form on the surface of the bottle. Another mechanism to obtain local supersaturation is when a reaction produces gas in excess. Relevant industrial applications are in the field of bio-reactors, such as fermenters for the production of bio-ethanol, where gaseous CO_2 is produced, or in electrolytic processes where gas (such as H_2 in the electrolysis of brine) bubbles are formed on the electrodes (Volanschi *et al.*, 1996). Models describing phase transition are very relevant for industry, but still lacking in practice.

The aim of this work is to give a starting point for Eularian-Lagrangian simulations of large scale bubbly flows where phase transition occurs. In the following sections, the used model and the numerical setup will be described and verified. Then, an outline of bubble formation due to supersaturation by heterogeneous nucleation will be given.

MODEL DESCRIPTION

The Discrete Bubble Model (DBM) is an Euler-Lagrange CFD model which is based on the work of Delnoij *et al.* (1999) subsequently expanded and improved by Darmana *et al.* (2005) and Lau *et al.* (2014). The model tracks each bubble separately using Newton's laws of motion and accounts for bubble-bubble interactions (collisions, coalescences and breakups), mass transport and it has been expanded in this work to account for phase transition. A detailed description of the model will be given in the following sections. For more details the reader can refer to the aforementioned works.

Hydrodynamics modeling

The fluid flow is described by the volume-averaged Navier-Stokes equations:

$$\frac{\partial}{\partial t}\left(\rho_l\alpha_l\mathbf{u}\right)+\nabla\cdot\left(\rho_l\alpha_l\mathbf{u}\mathbf{u}\right)=-\alpha_l\nabla p+\alpha_l\rho\mathbf{g}$$
$$+\nabla\cdot\alpha_l\boldsymbol{\tau}_l+\Phi \quad (1a)$$

$$\frac{\partial}{\partial t}\left(\rho_l\alpha_l\right)+\nabla\cdot\rho_l\alpha_l\mathbf{u}=\dot{M} \quad (1b)$$

where $\mathbf{u}$ is the fluid velocity, α_l denotes the liquid fraction and Φ represents the momentum coupling between the liquid and the discrete gas phase. In this equation $\boldsymbol{\tau}$ represents the stress tensor, which is the described with the very well known Equation 2 for Newtonian fluids.

$$\boldsymbol{\tau}_l=-\mu_{eff}\left[\nabla\mathbf{u}+(\nabla\mathbf{u})^T-\frac{2}{3}\boldsymbol{I}(\nabla\cdot\mathbf{u})\right] \quad (2)$$

The effective viscosity considers the contribution of the LES sub-grid scale turbulent viscosity, which is calculated using the model developed by Vreman (2004).

Bubble dynamics

Each individual bubble is tracked using Newton's law of motion accounting for the forces that the bubble experiences. For a spherical incompressible bubble, its motion is described as:

$$\rho_b V_b\frac{d\mathbf{v}}{dt}=\sum\mathbf{F}-\left(\rho_b\frac{dV_b}{dt}\right)\mathbf{v} \quad (3)$$

where $\mathbf{v}$ represents the bubble velocity. The sum of the forces on bubbles is composed of drag (Roghair *et al.*, 2011), lift (Tomiyama *et al.*, 2002), buoyancy, virtual mass (Auton, 1987) and wall-interactions (Tomiyama *et al.*, 1995), as given by Equation 4:

$$\sum\mathbf{F}=\mathbf{F}_G+\mathbf{F}_P+\mathbf{F}_D+\mathbf{F}_L+\mathbf{F}_{VM}+\mathbf{F}_W \quad (4)$$

The description of the forces considered is given in Table 1. The interphase coupling is performed through polynomial mapping, to transfer information from the discrete phase to the Eulerian grid and vice versa. The choosen technique is a clipped fourth-order polynomial following the work of Deen *et al.* (2004).

An important aspect is the volume change due to the interphase mass transfer. This is accounted for as:

$$\rho_b\frac{dV_b}{dt}=\dot{m} \quad (5)$$

More details on the mass transfer will be given in the following sections.

Bubble interactions

Bubble collisions, coalescence and breakup have been taken into account in the model. Since each bubble position, velocity and size are readily available as part of the solution, bubble encounters (with other bubbles or with a wall) are relatively easy to track. The collision model used in this work is based on the hard-sphere approach of Hoomans *et al.* (1996). The (binary) encounters are event-based and are treated as perfectly elastic collisions, unless coalescence takes place. To speed up the collision routines, a neighbour list concept as described by Darmana *et al.* (2005) is used. Since collisions are perfectly elastic, the tangential velocity component is not altered by the encounter while the normal component (assuming bubbles *i* and *j* collide) is calculated as:

$$v_{n,i}^{new}=2\frac{m_i v_{n,i}+m_j v_{n,j}}{m_i+m_j}-v_{n,i} \quad (6)$$

In performing the collision, the shrinkage or growth of bubbles as a consequence of mass transfer needs to be considered; in some specific cases the two elements are slowly diverging from each other but a collision can still take place if the radius is growing. In this case, the velocity sign should not be changed as the two bubbles are already diverging.

In addition to elastic collisions, bubbles can coalesce when sufficiently long in contact. Many theories and models exist on bubble coalescence (see Lau *et al.* (2014)). In this work the film drainage model as implemented by Darmana *et al.* (2005) is used. When two bubbles are colliding, they will coalesce if the contact time is larger than the time that it takes for the thin film of liquid trapped between them to drain (see Equation 7 and 8).

$$t_{contact}\geq t_{drainage} \quad (7)$$

Table 1: Forces acting on a bubble

Force	Closure relation
$\mathbf{F}_G = \rho_b V_b \mathbf{g}$	-
$\mathbf{F}_P = -V_b \nabla P$	-
$\mathbf{F}_D = -\frac{1}{2} C_D \rho_l \pi R_b^2 \|\mathbf{v} - \mathbf{u}\| (\mathbf{v} - \mathbf{u})$	$\frac{C_D}{C_{D,\infty}} = \left(1 + \frac{18}{E\ddot{o}} \alpha_b\right) \alpha_l$ $C_{D,\infty} = \sqrt{C_{D,\infty}(\text{Re})^2 + C_{D,\infty}(E\ddot{o})^2}$ $C_{D,\infty}(\text{Re}) = \frac{16}{\text{Re}}\left(1 + \frac{1}{1 + \frac{16}{\text{Re}} + \frac{3.315}{\sqrt{\text{Re}}}}\right)$ $C_{D,\infty}(E\ddot{o}) = \frac{4E\ddot{o}}{E\ddot{o} + 9.5}$
$\mathbf{F}_L = -C_L \rho_l V_b (\mathbf{v} - \mathbf{u}) \times (\nabla \times \mathbf{u})$	$C_L = \begin{cases} \min[0.288\tanh(0.121\text{Re}), f(E\ddot{o}_d)] & E\ddot{o} < 4 \\ f(E\ddot{o}_d) & 4 \leq E\ddot{o} \leq 10 \\ -0.29 & E\ddot{o} > 10 \end{cases}$ $f(E\ddot{o}_d) = 0.00105E\ddot{o}_d^3 - 0.0159E\ddot{o}_d^2 - 0.0204E\ddot{o}_d + 0.474$ $E\ddot{o}_d = \frac{E\ddot{o}}{E_b}, \quad E_b = \frac{1}{1 + 0.163E\ddot{o}^{0.757}}$
$\mathbf{F}_{VM} = -C_{VM} \rho_l V_b \left(\frac{D\mathbf{v}}{Dt} - \frac{D\mathbf{u}}{Dt}\right)$	$C_{VM} = 0.5$
$\mathbf{F}_W = -C_W R_b \left(\frac{1}{y^2} - \frac{1}{(L-y)^2}\right) \rho_l \|(\mathbf{v} - \mathbf{u}) \cdot \mathbf{n}_z\|^2 \mathbf{n}_w$	$C_W = \begin{cases} e^{(-0.933E\ddot{o} + 0.179)} & 1 \leq E\ddot{o} \leq 5 \\ 0.007E\ddot{o} + 0.04 & 5 \leq E\ddot{o} \leq 33 \end{cases}$

Prince and Blanch (1990) calculated the drainage time as:

$$t_{drainage} = \sqrt{\frac{d_{eq}^3 \rho_l}{128\sigma}} \ln\frac{\theta_0}{\theta_f} \tag{8}$$

where θ_0 and θ_f represents respectively the initial and final film thickness during the drainage process, which are equal to 1×10^{-4} m and 1×10^{-8} m respectively (Darmana *et al.*, 2005). Since the velocities and the sizes of each colliding couple are available, it is possible to calculate the contact time as proposed by Sommerfeld *et al.* (2003), assuming that it is proportional to a deformation distance divided by the normal component of the two bubbles' velocities:

$$t_{contact} = \frac{C_{co} d_{eq}}{2 |v_{n,i} - v_{n,j}|} \tag{9}$$

The coalescence constant (C_{co}) represents the deformation distance normalized by the effective bubble diameter. To conclude, for each pair of colliding bubbles it is possible to calculate both of the times and check whether a collision or a coalescence takes place. In the latter event, the resulting bubble will have a volume equal to the sum of the two parents.

Together with binary interactions between bubbles, a break-up model (described by Lau *et al.* (2014)) is implemented in the DBM. This model assumes that break-up occurs when the inertial forces acting on the bubble (which deform the bubble) are higher than the surface tension force. The break-up criterion is described in the form of a critical Weber number as (for spherical bubbles):

$$\text{We} = \frac{\rho_l (v_{n,i} - v_{n,j})^2 d_{eq}}{\sigma} \geq 12 \tag{10}$$

The daughter bubbles sizes are described by a U shaped daughter size distribution; since the location of the bubble is necessary for the DBM, it is assumed that it coincides with the parent for the largest bubble while the smaller is located randomly in the proximity of the other, avoiding immediate subsequent coalescence (see Lau *et al.* (2014).

Species transport and mass transfer

The DBM includes species transport, mass transfer and reaction (Darmana *et al.*, 2005). A transport equation for each species is implemented as:

$$\frac{\partial}{\partial t}\left(\alpha_l \rho_l Y_l^j\right) + \nabla\left(\alpha_l\left(\rho_l \mathbf{u} Y_l^j - \Gamma_{eff}^j \nabla Y_l^j\right)\right) = \dot{M} + \alpha_l S^j \tag{11}$$

where S^j represents the source/sink term accounting for chemical reactions and Γ_{eff} is calculated as:

$$\Gamma_{eff}^j = \rho_l \mathcal{D}_l^j + \frac{\mu_T}{Sc_T^j} \tag{12}$$

where the turbulent Schmidt number is approximated to $Sc_T^j = 1$ (Jain *et al.*, 2015). The transport equations are solved for N-1 components, while the last component is solved enforcing the summation equation:

$$\sum_{j=1}^{N_S} Y_l^j = 1 \tag{13}$$

The physical properties of the mixture are calculated as the weighted average of each specie. The interphase mass transfer is a function of the concentration difference between the bubble (assumed to be composed entirely of one gas, namely CO_2) and the liquid. This has been expressed by (Darmana *et al.*, 2005) as:

$$\dot{m}_b^j = k_l^j A_b \rho_l \left(Y_l^{j*} - Y_l^j\right) \tag{14}$$

The mass transfer coefficient is determined by a Sherwood relation (Bird *et al.*, 2007):

$$Sh = 2 + 0.6415(ReSc^j)^{1/2} \tag{15}$$

The gas side mass fraction is calculated from the Henry constant:

$$Y_l^{j*} = H^j Y_b^j \frac{\rho_b}{\rho_l} \tag{16}$$

The transport equation is discretized implicitly (with a semi-implicit source term for the reaction) on the Eulerian grid and the resulting linear system is solved using a biconjugate gradient method implemented in the scientific library PETSc (Balay *et al.*, 2016, 1997).

Verification

The hydrodynamics of the DBM has been verified in the past by Lau *et al.* (2014), with the use of experimental data from a square bubble column, performed by Deen *et al.* (2001). On the other hand, the species solver has been modified since Darmana *et al.* (2005) and a verification is requried to assess the numerical validity of the results. A few unidirectional validation cases have been performed, as will be detailed in the following sections.
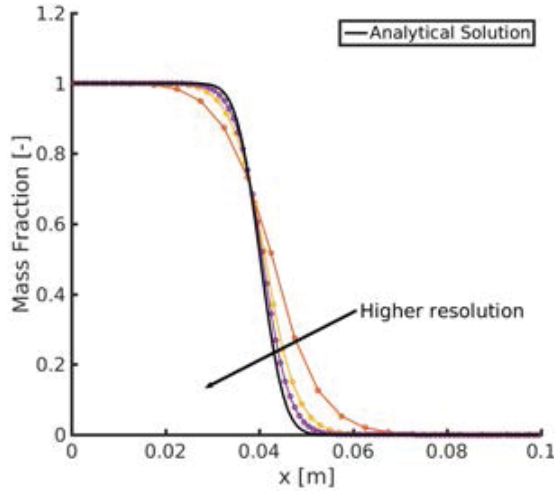

Figure 1: Comparison of the DBM species solver with the analytical solution for a unidirectional convection-diffusion flow, for different grid resolutions. The analytical solution is represented by the black line.

1D convection-diffusion

In this case, a unidirectional flow in the domain is considered where the concentration of the component of interest is initially zero. The density is assumed constant. A flow from one side (where the mass fraction is $Y_l = 1$) is started and diffusion takes place. Equation 11 simplifies to:

$$\frac{\partial c}{\partial t} + u\frac{\partial c}{\partial x} = \mathcal{D}\frac{\partial^2 c}{\partial x^2} \tag{17}$$

The analytical solution for this system has been derived by Ogata and Banks (1961) as:

$$\frac{c}{c_0} = \frac{1}{2}\left[\text{erfc}\left(\frac{x-ut}{2\sqrt{\mathcal{D}t}}\right) + \exp\left(\frac{ux}{\mathcal{D}}\right)\text{erfc}\left(\frac{x+ut}{2\sqrt{\mathcal{D}t}}\right)\right] \tag{18}$$

It is visible that the grid resolution plays an important role (due to the well known numerical diffusion) but the solver apporaches very well the analytical solution at high enough (100 in this case) number of grid elements.

Batch reaction

It is very important to verify the correct implementation of the semi-implicit discretization for the source/sink term and mass transfer. A simple reaction $A \rightarrow B$ is implemented with a first and a second order kinetics, asssuming an ideally mixed batch reactor. In this case, Equation 11 simplifies to:

$$\frac{dc}{dt} = R = \begin{cases} -k_R c & 1^{st} \text{ order reaction} \\ -k_R c^2 & 2^{nd} \text{ order reaction} \end{cases} \tag{19}$$
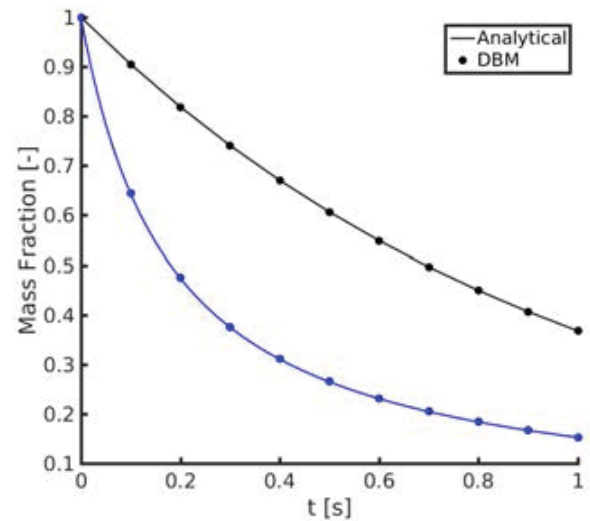

Figure 2: First (top line) and second (bottom line) order reactions in a batch reactor: comparison with the analytical solutions.

where k_R represents the reaction rate. Integration of Equation 19 yields to the analytical solutions:

$$c = \begin{cases} c_0\exp(-k_R t) & 1^{st} \text{ order reaction} \\ \frac{1}{1/c_0+k_R t} & 2^{nd} \text{ order reaction} \end{cases} \tag{20}$$

As shown in Figure 2, the DBM results match very well with the analytical solutions.

Phase transition

Theoretical overview

An important concept is supersaturation: a liquid is (locally) supersaturated when the concentration is higher than the equilibrium concentration, which can be expressed, for instance, by Henry's law as done in Equation 16. A relevant parameter, called the *supersaturation ratio*, is introduced as (Enríquez *et al.*, 2013):

$$\zeta = \frac{c}{c_s} - 1 \tag{21}$$

It is visible that, for phase transition to occur, $\zeta > 0$. The equilibrium condition is when this ratio is equal to 0.

The mechanism of a gas bubble formation is not new in literature (Jones *et al.*, 1999). Several possible ways are accounted for, where two different classes are distinguished: homogeneous and heterogeneous nucleation. The first occurs when a bubble is formed, together with a completely new interface, anywhere in the liquid bulk where supersaturation exists. However, the energy barrier required for this mechanism to occur is high, so that homogeneous nucleation happens only when the supersaturation ratio is extremely large, as for $\zeta > 1000$ (Wilt, 1986). On the other hand, the supersaturation of common drinks like soda and champagne reaches much lower levels of ζ, which is in the order of ~2 to 5 (Enríquez *et al.*, 2013; Liger-Belair *et al.*, 2002). For this case, bubbles are forming in large numbers via heterogeneous nucleation. This mechanism describes the formation of gas bubbles on so-called *nucleation sites*, such as impurities in the liquid bulk, small cavities on the container or other gas bubbles. In those sites, a gas-pocket can be easily

formed and grow. The size of the nucleation site is crucial in describing the formation and growth of a bubble, as it determines whether a bubble will grow or be dissolved back into the liquid. Only nucleation sites with a radius larger than a critical value (related to the Laplace pressure) can host a growing bubble:

$$R_c = \frac{2\sigma}{p_s\zeta} \tag{22}$$

Implementation in the DBM

The DBM has been extended to account for local supersaturation. For every Eulerian grid cell, the local supersaturation ratio is calculated, as described by Equation 21. It is then possible to calculate the local critical radius (see Equation 22), which represents the minimal size a bubble should have in order to grow and not dissolve again. Since the volume of the Eulerian cell is known as well as ζ, it is possible to calculate the excess mass (or volume) of gas which is present in each cell. From this, the volume of a possible nucleated bubble it is easily derived and compared to the critical radius. If the candidate bubble is large enough, it is generated (and the transferred mass is accounted for as described in the previous sections) with the critical radius and randomly placed in the cell, avoiding possible overlaps with neighbouring bubbles. An important limitation to this is that a single bubble is created for every cell (since the preferred way to reduce the supersaturation is mass transfer to neighbouring bubbles) which makes it depending on the grid size. Research is currently ongoing to study, with the help of experiments, bubble formation rates and how to link them to the DBM in a Lagrangian manner (such as discrete nucleation sites with their own properties as size or contact angle).

RESULTS

Numerical setup

The considered domain is a square box of 15 cm described by an Eulerian grid of $30 \times 30 \times 30$ grid nodes. The liquid is water and its properties are at standard conditions ($\rho_l = 1000\,\mathrm{kg\,m^{-3}}$, $\sigma = 0.073\,\mathrm{N\,m^{-1}}$ and $\mu_l = 10^{-3}\,\mathrm{Pa\,s}$). The dissolved gas is CO_2, which is perfectly mixed in the liquid bulk with a mass fraction of $Y_{CO_2} = 0.003$, corresponding to an initial supersaturation ratio $\zeta = 0.783$. This has been arbitrarily chosen to avoid forming very small or very large bubbles. The typical time step is 1 ms for both the species and the flow solvers while bubbles moves at a pace 20 times smaller. Two different mechanisms have been implemented, heterogeneous nucleation on the bottom surface and nucleation in the liquid bulk. Even though it has been already explained that the predominant mechanism for bubble nucleation is the first, it is still worth to do a comparison between the two as, in principle, a bubble can use a nucleation site which is suspended in the liquid such as solid impurities.

Bubble formation

*Heterogeneous nucleation on a surface*

In this implementation, bubbles are forced to form only in the lower plane of the box, which represents a solid surface. In the bottom plane (represented in this case by all the grid cells in the x and y directions with z between 0 and Δz), each bubble is generated with a random position in all directions in order to avoid overlap with walls and/or other neighbouring bubbles. As shown in Figure 3, small bubbles are formed at the bottom plane, which immediately start rising and increase their size due to mass transfer and coalescence. A
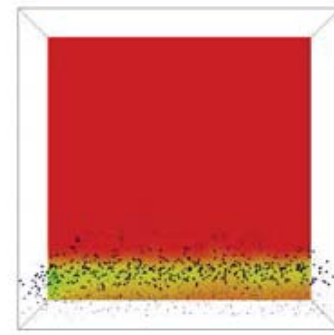
(a) $t = 0.65\,\mathrm{s}$
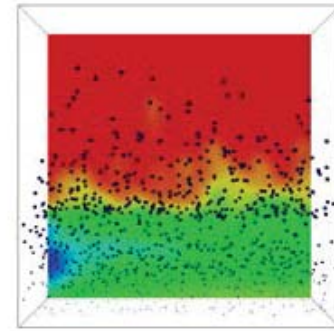
(b) $t = 1.15\,\mathrm{s}$
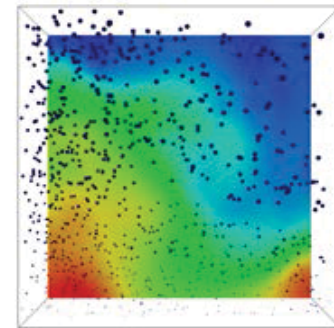
(c) $t = 7.5\,\mathrm{s}$

Figure 3: Snapshots of the concentration profiles around bubbles for the surface nucleation case. The color range from higher dissolved gas concentration (red) to lower (blue).

bubble front is formed in the first time steps, due to the initialization technique. After the startup of the phase transition, bubbles induce mixing with strong circulation patterns (see Figure 3c) and the lower concentration area shifts to the top, as expected since bubbles are rising upwards and the dissolved gas is transfered to them. In Figure 3c a large vortex is visible, induced by the bubble movement.

Heterogeneous nucleation in the liquid bulk

In this case bubbles are free to nucleate in the whole domain, mimicking a liquid which contains enough solid impurities that act as nucleation sites. As a consequence, at the first time step a large (equal to the number of grid elements) number of bubbles are formed (see Figure 4). It is noticeable how, at first, smaller bubbles are formed all over the bulk but later, as a consequence of mass transfer, the average size is consider-
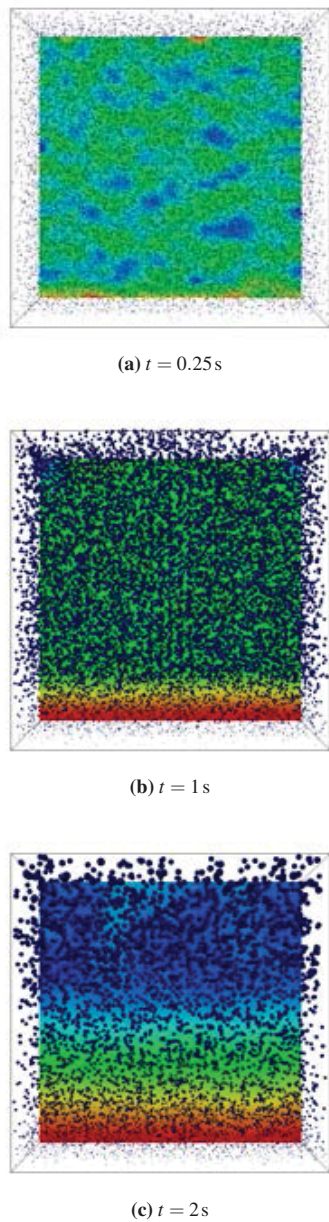
(a) $t = 0.25\,\mathrm{s}$

(b) $t = 1\,\mathrm{s}$

(c) $t = 2\,\mathrm{s}$

Figure 4: Snapshots of the concentration profiles around bubbles for the bulk nucleation case. The color range from higher dissolved gas concentration (red) to lower (blue).

Figure 5: Comparison of the average bubble diameter in the column for the two cases: Case 1 nucleation on a surface and Case 2 in the liquid bulk.

Figure 6: Comparison of the bubble density in the column for the two cases: Case 1 nucleation on a surface and Case 2 in the liquid bulk.

ably higher at the top of the domain, similarly to the previous case. Also in this case, a concentration front which goes from the bottom to the top can be clearly discerned, following the direction of the rising bubbles. In this situation, it appears that the bubbles create less vortices, probably because they are distributed more uniformly throughout the domain.

Comparison

A comparison of the bubble diameter is shown in Figure 5. It is immediately clear that the average diameter is at first the same, because the supersaturation ratio ζ is the same and thus bubbles are formed with an equal size. Despite the bubble numbers are clearly not the same (see Figure 6 for a comparison) and a large number of small bubbles is formed for the nucleation in the liquid bulk, the two profiles for the average bubble diameter follow the same trends. At the startup, the
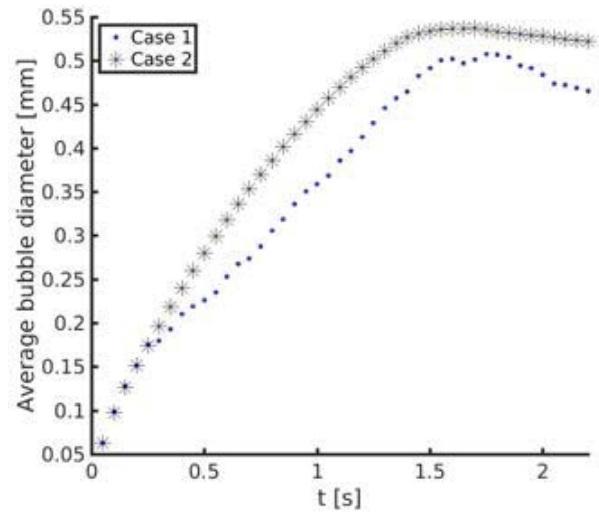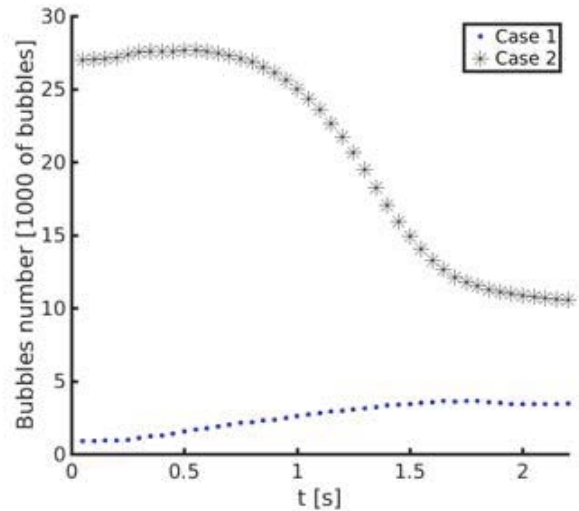
bubble size is small and immediately starts to increase as a consequence of mass transfer but even more importantly of coalescence. Since more bubbles are present in the second case, they have a higher probability to coalesce, leading to a slightly larger average bubble size.

A comparison of the bubble numbers is provided in Figure 6. It is particularly interesting to notice the opposite behaviour of the two cases. While for the second case the, at first large, number of bubbles is reduced, the other case sees an increase. This can be explained by the effect of coalescence for the second case, which also explains the larger average bubble diameter. In addition, a second effect contributes to the difference: in the second case bubbles are not free anymore to nucleate, because most of the cells already contain a bubble. In the second case, on the other hand, the domain is almost empty and, as soon as the first bubbles leave the bottom plane, new bubbles will form while the others are still in

the domain.

CONCLUDING REMARKS

This work represents a starting point to model bubble formation in a liquid. A first algorithm has been set up to study the formation of bubbles both on a solid surface and in the liquid bulk. The choice of the bubble formation mechanism has a large influence in determining the bubble numbers, which are consistently larger for the bulk nucleation case. Moreover, the concentration front shows a different behaviour for the first case, where it shifts from a lower concentration at the bottom to the opposite situation. In addition, bubble sizes are also changed, as a consequence of coalescence.

However, this model is not yet complete. Currently, we are working on expanding the model to account for Lagrangian nucleation sites, where with mass transfer a bubble can grow and detach, avoiding the influence of the grid size. Moreover, an experimental setup is under construction to first study nucleation rates, bubble numbers and sizes at an intermediate scale and eventually validate the results of the DBM. To conclude, the inclusion of phase transition as a consequence of superheating (boiling case) will also be considered.

AKNOWLEDGEMENTS

REFERENCES

AUTON, T.R. (1987). "The lift force on a spherical rotational flow". *J. Fluid Mech*, **183**, 199–218.

BALAY, S., GROPP, W.D., MCINNES, L.C. and SMITH, B.F. (1997). "Efficient Management of Parallelism in Object Oriented Numerical Software Libraries". E. Arge, A.M. Bruaset and H.P. Langtangen (eds.), *Modern Software Tools in Scientific Computing*, 163–202. Birkhäuser Press.

BALAY, S., ABHYANKAR, S., ADAMS, M.F., BROWN, J., BRUNE, P., BUSCHELMAN, K., DALCIN, L., EIJKHOUT, V., GROPP, W.D., KAUSHIK, D., KNEPLEY, M.G., MCINNES, L.C., RUPP, K., SMITH, B.F., ZAMPINI, S., ZHANG, H. and ZHANG, H. (2016). "PETSc Users Manual". Tech. Rep. ANL-95/11 - Revision 3.7, Argonne National Laboratory.

BIRD, R.B., STEWART, W.E. and LIGHTFOOT, E.N. (2007). *Transport Phenomena*. Revised 2n ed. John Wiley & Sons, New York.

DARMANA, D., DEEN, N.G. and KUIPERS, J.A.M. (2005). "Detailed modeling of hydrodynamics, mass transfer and chemical reactions in a bubble column using a discrete bubble model". *Chemical Engineering Science*, **60(12)**, 3383–3404.

DEEN, N.G., SOLBERG, T. and HJERTAGER, B.H. (2001). "Large eddy simulation of the Gas-Liquid flow in a square cross-sectioned bubble column". *Chemical Engineering Science*, **56(21)**, 6341–6349.

DEEN, N.G., VAN SINT ANNALAND, M. and KUIPERS, J.A.M. (2004). "Multi-scale modeling of dispersed gas-liquid two-phase flow". *Chem. Eng. Sci.*, **59(8-9)**, 1853–1861.

DELNOIJ, E., KUIPERS, J.A.M. and VAN SWAAIJ, W.P.M. (1999). "A three-dimensional CFD model for gas-liquid bubble columns". *Chemical Engineering Science*, **54(13-14)**, 2217–2226.

ENRÍQUEZ, O.R., HUMMELINK, C., BRUGGERT, G.W., LOHSE, D., PROSPERETTI, A., VAN DER MEER, D. and SUN, C. (2013). "Growing bubbles in a slightly supersaturated liquid solution". *Review of Scientific Instruments*, **84**, 065111.

HOOMANS, B.P.B., KUIPERS, J.A.M., BRIELS, W.J. and VAN SWAAIJ, W.P.M. (1996). "Discrete particle simulation of bubble and slug formation in a two-dimensional gas-fluidised bed: A hard-sphere approach". *Chemical Engineering Science*, **51(1)**, 99–118.

JAIN, D., DEEN, N.G. and KUIPERS, J.A.M. (2015). "Numerical modeling of carbon dioxide chemisorption in sodium hydroxide solution in a micro-structured bubble column". *Chem. Eng. Sci.*, **137**, 685–696.

JONES, S.F., EVANS, G.M. and GALVIN, K.P. (1999). "Bubble nucleation from gas cavities - a review". *Advances in Colloid and Interface Science*, **80(1)**, 27–50.

LAU, Y.M., BAI, W., DEEN, N.G. and KUIPERS, J.A.M. (2014). "Numerical study of bubble break-up in bubbly flows using a deterministic Euler-Lagrange framework". *Chemical Engineering Science*, **108**, 9–22.

LIGER-BELAIR, G., VIGNES-ADLER, M., VOISIN, C., Bertrand Robillard and JEANDET, P. (2002). "Kinetics of Gas Discharging in a Glass of Champagne: The Role of Nucleation Sites". *Langmuir*, **18(4)**, 1294–1301.

OGATA, A. and BANKS, R.B. (1961). "A solution of the differential equation of longitudinal dispersion in porous media". Tech. rep.

PRINCE, M.J. and BLANCH, H.W. (1990). "Bubble coalescence and break-up in air-sparged bubble columns". *AIChE Journal*, **36(10)**, 1485–1499.

ROGHAIR, I., LAU, Y.M., DEEN, N.G., SLAGTER, H.M., BALTUSSEN, M.W., VAN SINT ANNALAND, M. and KUIPERS, J.A.M. (2011). "On the drag force of bubbles in bubble swarms at intermediate and high Reynolds numbers". *Chemical Engineering Science*, **66(14)**, 3204–3211.

SOMMERFELD, M., BOURLOUTSKI, E. and BRÖDER, D. (2003). "Euler/Lagrange Calculations of Bubbly Flows with Consideration of Bubble Coalescence". *The Canadian Journal of Chemical Engineering*, **81(3-4)**, 508–518.

TOMIYAMA, A., MATSUOKA, T., FUKUDA, T. and SAKAGUCHI, T. (1995). "A Simple Numerical Method for Solving an Incompressible Two-Fluid Model in a General Curvilinear Coordinate System". *Multiphase Flow 1995*, 241–252.

TOMIYAMA, A., TAMAI, H., ZUN, I. and HOSOKAWA, S. (2002). "Transverse migration of single bubbles in simple shear flows". *Chemical Engineering Science*, **57(11)**, 1849–1858.

VAN SINT ANNALAND, M., DEEN, N.G. and KUIPERS, J.A.M. (2003). *Multi-level modeling of dispersed gas-liquid two-phase flows*. Heat and mass transfer. Springer, Berlin.

VOLANSCHI, A., OUDEJANS, D., OLTHUIS, W. and BERGVELD, P. (1996). "Gas phase nucleation core electrodes for the electrolytical method of measuring the dynamic surface tension in aqueous solutions". *Sensors and Actuators B*, **35-36**, 73–79.

VREMAN, A.W. (2004). "An eddy-viscosity subgrid-scale model for turbulent shear flow: Algebraic theory and

applications". *Physics of Fluids*, **16(10)**, 3670–3681.

WILT, P.M. (1986). "Nucleation rates and bubble stability in water-carbon dioxide solutions". *Journal of Colloid and Interface Science*, **112(2)**, 530–538.